Journal of Alloys and Compounds 973 (2024) 172938

Contents lists available at ScienceDirect

Journal of Alloys and Compounds

journal homepage: www.elsevier.com/locate/jalcom

Tunable magnetocaloric effect towards cryogenic range by varying Mn:Ni ratio in all-d-metal Ni(Co)-Mn-Ti Heusler alloys

Aun N. Khan, Álvaro Díaz-García, Luis M. Moreno-Ramírez *, Jia Yan Law, Victorino Franco

Dpto. Física de la Materia Condensada. ICMS-CSIC. Universidad de Sevilla, P.O. Box 1065, Sevilla 41080, Spain

ARTICLE INFO

Keywords:
All-d-metal Heusler alloys
Ni(Co)-Mn-Ti
Magnetostructural transition
Magnetocaloric effect

ABSTRACT

Cryogenic magnetic refrigeration is a highly efficient and environmentally friendly technique for gas liquefaction. However, refrigerant materials undergoing large magnetocaloric response at the interesting cryogenic range are dominated by critical elements (mainly rare-earth elements) which impedes practical applicability of such refrigeration systems. Therefore, there is a need for dedicated investigations on optimization of magnetocaloric response at cryogenic range by utilizing compositions that are rare-earth free. In this work, we synthesize the mechanically stable and rare-earth free, all-d-metal $Ni_{35}Co_{15}Mn_{35}Ti_{15}$ Heusler alloys and investigate the role of varying Mn:Ni ratio on the magnetostructural and magnetocaloric properties of the alloy system. The results of the microstructural characterization indicate homogenous composition for the investigated alloy series. As the Mn:Ni ratio increases from 1.01 to 1.10, the martensitic transition shifts from near-room temperature down to cryogenic region (120–140 K) while the magnetization of the austenitic phase remains unaltered. Isothermal entropy change as high as ~ 13 J kg^{-1} K^{-1} at 1.5 T is achieved for the sample with the highest Mn:Ni ratio at the temperature region for natural gas liquefaction, which significantly surpasses the values previously reported in the literature for similar alloys. In addition to large magnetocaloric response, the martensitic transformation falls in an interesting temperature of the cryogenic region, paving the way for various low-temperature magnetocaloric applications.

1. Introduction

The quest to increase the energy efficiency and environmental friendliness of refrigeration processes stems from the global warming challenge that directly leads to an ever-growing demand for cooling appliances [1,2]. In addition to the need of refrigeration systems working around room temperature, there is also an increasingly demand for gas liquefaction (H_2, natural gas, etc.), which requires refrigeration systems functioning at cryogenic temperatures [3]. It is expected that the efficiency of such appliances can be substantially improved by utilizing systems based on the magnetocaloric effect (MCE) [1,4]. The MCE is defined as the temperature (entropy) change that a magnetic material shows when subjected to adiabatic (isothermal) magnetization/demagnetization processes. The effect is maximum when large magnetization changes with temperature and field occur, e.g. along a thermomagnetic phase transition. However, the search for magnetocaloric materials with a good compromise between criticality/cost, performance and mechanical stability is still ongoing. Magnetocaloric materials are currently classified according to their undergoing magnetic transition which can be either first-order (FOPT) or second-order (SOPT) [5]. These materials hold a key significance in the success of such emerging technology, with materials exhibiting FOPT attracting the most attention due to their larger MCE compared to SOPT ones [2]. Among the different families of FOPT materials, Heusler alloys exhibiting magnetostructural transformation (martensitic type) are placed as potential candidates for applications. However, further research is required as some intrinsic characteristics of this type of FOPT can have a relevant detrimental effect in working conditions. The main drawback in such materials is the associated thermal hysteresis which drastically decreases the reversible response and cannot be simply overcome by increasing the applied magnetic field [6–9]. In addition, poor mechanical stability in cyclic operating conditions due to successive volume changes during the transition can rapidly degrade their response and structural integrity due to the relatively weak grain boundary cohesion [10–12]. Compared to classic Heusler alloys, the newly reported all-d-metal Ni(Co)-Mn-Ti Heusler alloys show improved mechanical performance than those containing p-block elements while keeping an excellent magnetocaloric response [13,14].

* Corresponding author.
E-mail address: lmoreno6@us.es (L.M. Moreno-Ramírez).

https://doi.org/10.1016/j.jallcom.2023.172938
Received 12 July 2023; Received in revised form 7 November 2023; Accepted 20 November 2023
Available online 23 November 2023

Regarding cryogenic applications, the most promising magnetocaloric materials are the rare-earth containing such as the Laves-phase type RCo_2, RAl_2 and RNi_2 alloys (R = rare-earth element) and their solid solutions and composites [15–19]. However, the large-scale applicability of such refrigerant materials becomes limited due to the economic and environmental challenges which rare-earth elements impose. Criticality, which deals with the supply risk of the material together with its economic importance, is another vital parameter which determines large-scale applicability of a material [20]. A possible solution is to extend the applicability of well-known FOPT rare-earth free magnetocaloric materials for room-temperature applications downwards the cryogenic range by compositional modifications. Some attempts include the $(Mn,Fe)_2(P,Si)$ alloys for which the transition temperature can be tuned from 300 K to 99 K by varying both Mn:Fe and P:Si ratios, reaching a maximum isothermal entropy change of ~11 J kg^{-1} K^{-1} for an applied magnetic field of 2 T at 110 K [21]. Another promising class of FOPT materials for cryogenic applications are the La$(Fe,Si)_{13}$ alloys [22]. J. Lai *et al.* had successfully demonstrated that the transition temperature below 77 K can be reached by partially doping La by Ce and Fe by Mn [22]. MnTX alloys undergoing FOPT are also promising rare-earth free magnetocaloric materials, among them we highlight (Mn,Fe)Ni(Si,Al) compositions as they are based on abundant elements and show a tunable transition near-room temperature [23,24]. Regarding the promising Ni(Co)-Mn-Ti Heusler alloys, B. Beckmann *et al.* recently demonstrated that martensitic transition in the near-cryogenic temperature range is achievable for this alloy family by varying the Mn:Ti ratio [25]. Z. Guan *et al.* reported isothermal entropy changes up to ~ 16 J kg^{-1} K^{-1} for a large field values of 5 T at ~ 150 K [26]. However, further optimization is needed as large thermal hysteresis and relatively lower MCE as compared to that of rare-earth containing alloys still remains a real concern for the magnetic refrigerant materials exhibiting FOPT at cryogenic range.

In this work, we investigate the influence of significant variations of Mn:Ni ratio on the microstructure, martensitic transformation, and MCE in the parent $Ni_{35}Co_{15}Mn_{35}Ti_{15}$ Heusler alloys. Previous work has shown that Mn:Ni ratio can tune the magnetostructural and magnetocaloric properties of all-d-metal Ni(Co)-Mn-Ti Heusler alloys downwards lower temperatures with slight changes in composition. However, there is still room for improving the magnetocaloric response and to explore the cryogenic applicability of these compounds as the maximum entropy change reported is 11.3 J kg^{-1} K^{-1} for 5 T at 290 K [27]. It is found that with an increasing Mn:Ni ratio up to 1.10, the martensitic transformation decreases towards cryogenic temperatures (down to 120 K). The decrease in transition temperature is accompanied by a non-linear increase in the isothermal entropy change, reaching 13 J kg^{-1} K^{-1} for the sample with the highest Mn:Ni ratio at moderate magnetic fields of 1.5 T. This MCE response at the cryogenic temperature range is more promising than those previously reported for this family of alloys, showing more than 100% improvement in the isothermal entropy change and a 20% reduction in thermal hysteresis [25,26]. Furthermore, in comparison with rare-earth containing alloys [28–31], the MCE response for moderate field changes is significantly improved in the explored range together with an estimated criticality which is substantially low compared to that of rare-earth containing alloys.

It has been shown in this work that the novel strategy involving variation of Mn:Ni ratio in all-d-metal Ni(Co)-Mn-Ti Heusler alloys is viable and effective in shifting the martensitic transition temperatures from near-room temperature down to cryogenic temperature range without deteriorating the magnetocaloric response, while showcasing low criticality as compared to the rare-earth containing alloys, both of which play a vital role in practical applicability of these materials.

2. Materials and methods

The Mn:Ni ratio in the parent $Ni_{35}Co_{15}Mn_{35}Ti_{15}$ composition was systematically varied. The samples were initially synthesized by arc melting (Edmund Bühler MAM-1) starting from raw materials (at least 99.9% purity) in an argon-controlled atmosphere. The resulting ingots were remelted 3 times using induction melting (Edmund Bühler Copper boat) and flipped each time to ensure homogeneity. The as-cast ingots were annealed at 1273 K for 4 days followed by water quenching, which was established as optimal annealing protocol in previous works on all-d-metal Ni(Co)-Mn-Ti Heusler alloys [32,33].

Microstructure and composition were characterized using X-ray diffraction (XRD, Bruker D8I diffractometer with Cu-Kα radiation) and scanning electron microscopy equipped with energy dispersive X-ray spectrometry (SEM-EDX; FEI™ Teneo).

The samples have been designated according to the measured Mn:Ni ratio, with an error margin of 3% derived from the EDX measurements, such as, 1.01 (**S1**), 1.03 (**S2**), 1.05 (**S3**) and 1.10 (**S4**).

Temperature dependent isofield magnetization measurements, $M(T)$, were performed in a Lake Shore 7407 vibrating sample magnetometer (VSM) using a sweeping rate of ≈ 10 K min^{-1}. The isothermal entropy change, ΔS_{iso}, was indirectly obtained from isothermal magnetization measurements, $M(H)$, using a discrete approximation to the following equation [34,35]:

$$\Delta S_{iso} = \mu_0 \int_0^H \left(\frac{\partial M}{\partial T}\right)_{H'} dH', \tag{1}$$

where μ_0 is the magnetic permeability of vacuum, M the magnetization, T the temperature, and H the magnetic field. The different $M(H)$ curves were measured using a discontinuous protocol which resets the history of the samples prior each isothermal measurement in order to prevent the appearance of spurious results due to the hysteretic behavior in FOPT materials [36–38]. For example, for obtaining the ΔS_{iso} upon heating, the erasing temperature was established well below the transition (where the $M(T)$ plot shows no hysteresis). Subsequently, the sample was heated without field from the erasing temperature to the desired measuring temperature where the field was then increased in isothermal conditions. Needle-like samples were used (~ 3 mg each) to minimize the demagnetization factor and to have a negligible influence on the isothermal entropy change calculations [39]. To evaluate the magnetocaloric performance of the studied series, the temperature average entropy over a span (ΔT) of 5 K and 10 K, $TEC(5)$ and $TEC(10)$, were calculated using the following equation [40]:

$$TEC(\Delta T) = \frac{1}{\Delta T} \max \left\{ \int_{T-\Delta T}^{T+\Delta T} \Delta S_{iso}(T') dT' \right\} \tag{2}$$

3. Results and discussion

Fig. 1 shows the backscattered scanning electron (BSE) images combined with elemental mapping at room temperature taken on polished sample surfaces of the alloy series. The needle-like structures evident in the BSE images of **S1**, **S2,** and **S3** seem to correspond to the martensitic phase [32,41]. The large parallel variants of martensite are rather evident in **S1**. In contrast, the growth of martensitic variants is slightly hindered for **S2** and became subtle for **S3**. Whereas no evidence of needle-like structure is found for **S4**. Elemental mapping analysis reveals a homogeneous composition for the series, confirming that the dark and bright regions observed in the BSE images do not correspond to compositional contrast [42]. The composition of the alloys obtained by EDX analysis is drawn in Fig. 2.

It can be observed from Fig. 2 that the Mn content increases from **S1** to **S4** while the Ni content is reduced according to the nominal compositions. This leads to the desired Mn:Ni ratio variation through the series. According to these results, the obtained Mn:Ni ratios are found to be 1.01 for **S1**, 1.03 for **S2**, 1.05 for **S3** and 1.10 for **S4**, with an error margin of 3% derived from the EDX measurements. The Co and Ti content remains relatively constant (all the measured contents are

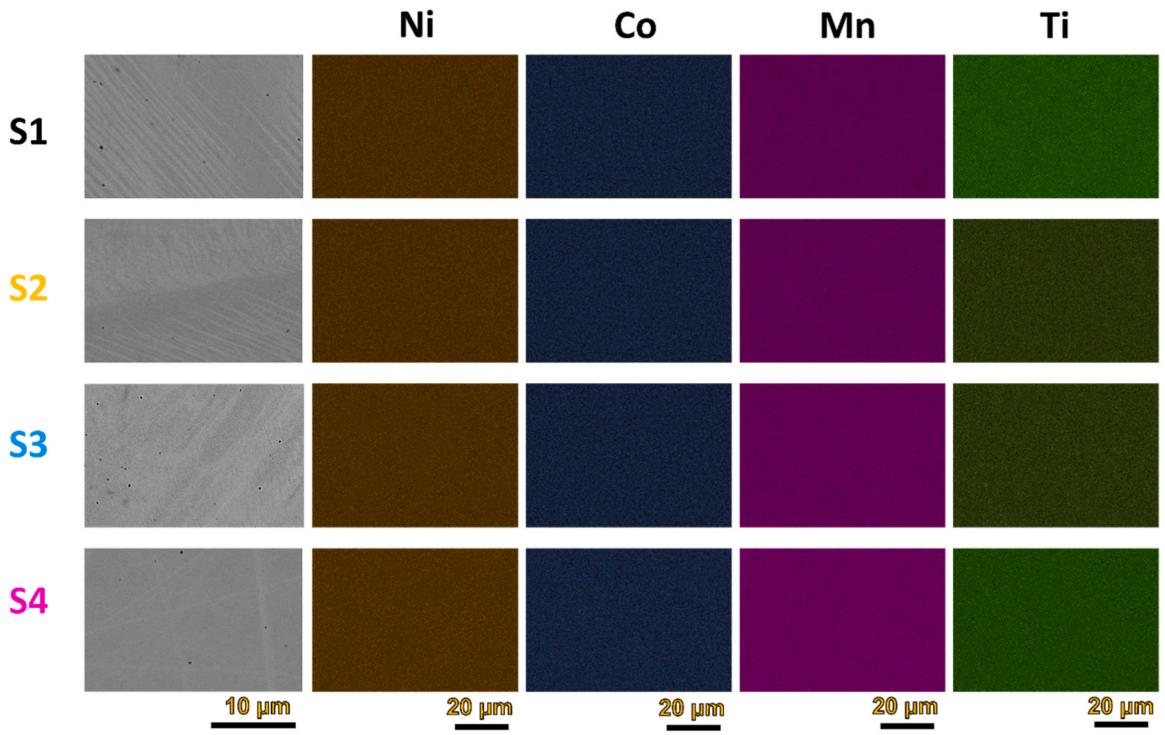

Fig. 1. Backscattered scanning electron (BSE) images (first column) and elemental mapping for the studied alloy series.

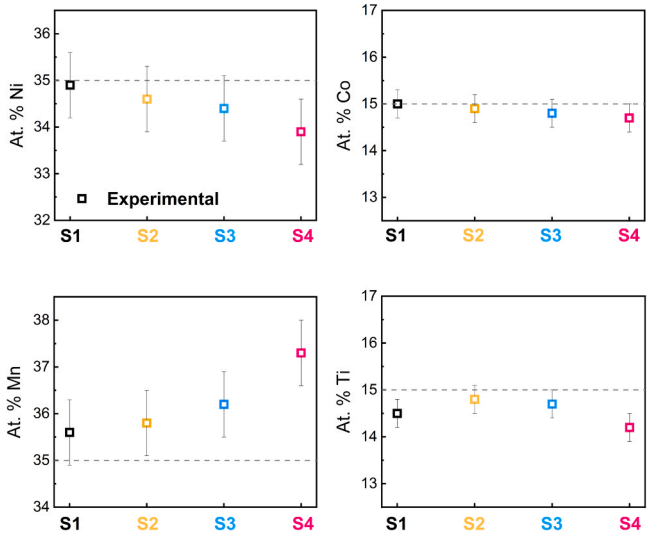

Fig. 2. Obtained composition from EDS analysis: (a) Ni, (b) Co, (c) Mn, and (d) Ti. Dashed lines indicate the parent composition.

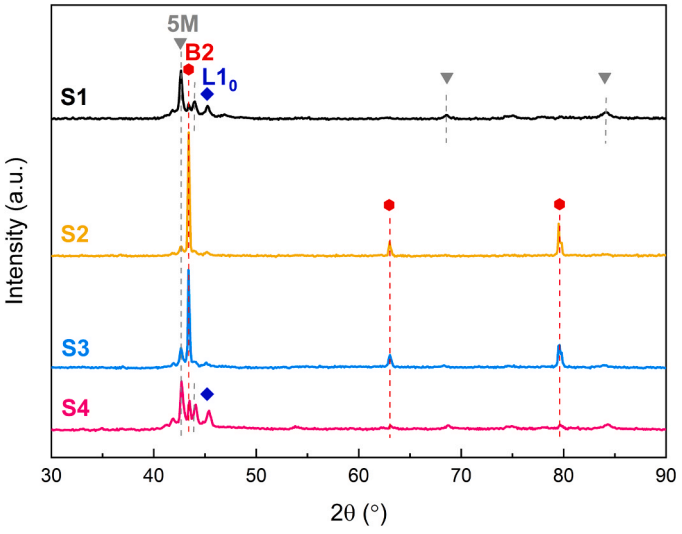

Fig. 3. Room temperature powder XRD spectra for the studied series. Indexed peaks for 5 M (grey lines) B2 (red lines) and $L1_0$ (blue) structures.

within the error margin of the measurements which is around 2%). All the obtained compositions are close to the expected ones and only the Ti content is slightly deviated for all the samples (~ 3% smaller from the desired value of 15 at%).

The room temperature powder XRD analysis is used to obtain useful insights about the different phases present in the studied alloy series, with the patterns depicted in Fig. 3. For **S1**, a mixture of modulated 5 M martensite (indexed by grey lines) and cubic B2 austenite (indexed by red lines) is observed along with small amounts of $L1_0$ phase (which is presented in all the samples). In accordance with the BSE analysis, an increase in the Mn:Ni ratio from **S1** to **S3** shifts the transition towards higher fractions of cubic B2 austenite. However, compared to **S2** and **S3**, **S4** shows pattern which resembles that of **S1** with a relevant amount of modulated 5 M martensite at room temperature. This seems to be counterintuitive according to previous BSE analysis. However, it should be considered that the grinding process for powder XRD measurements can change the structural and thermomagnetic behavior of Ni-Mn based alloys [43]. In the subsequent section, this effect will be further discussed.

Fig. 4**a** shows the temperature dependence of magnetization, $M(T)$ plots, for the alloy series for an applied field of 1 T. Upon heating, all samples show a significant magnetization increase which is related to the magnetostructural transition from low temperature martensitic phase to high temperature austenite with higher magnetization. This abrupt magnetization increase is followed by a gradual decrease in magnetization due to the Curie transition of the austenitic phase. Upon

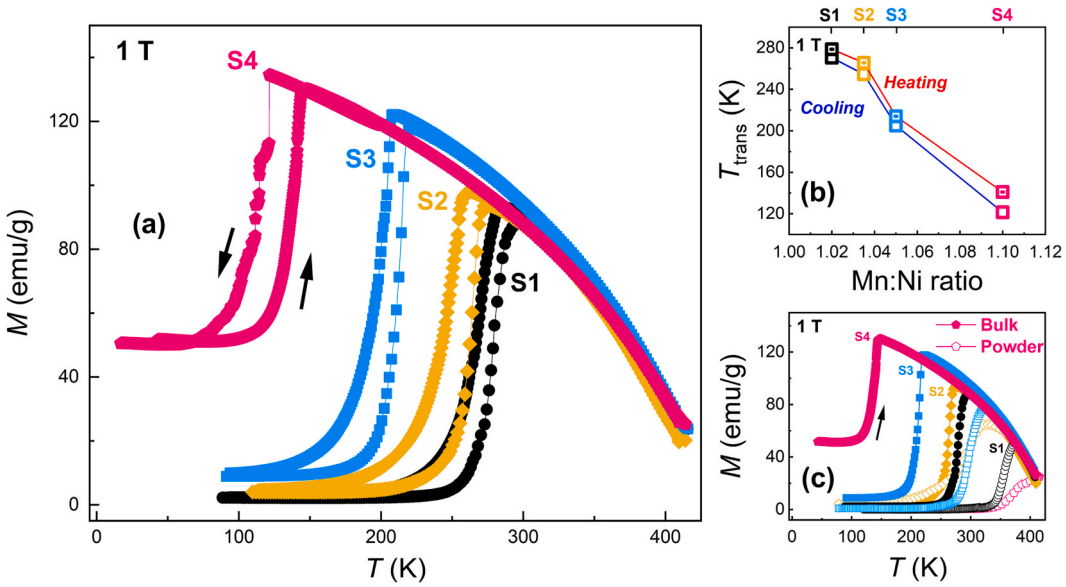

Fig. 4. (a) Temperature dependence of magnetization for 1 T (b) martensitic transition temperatures for heating (red line) and cooling (blue line) and (c) $M(T)$ plots upon heating for bulk and powder samples at 1 T.

cooling, the magnetization coincides with the heating path due to the absence of hysteresis in the Curie transition of the austenite. However, the cooling branch of the magnetostructural transition is shifted to lower temperature compared to the heating one due to the characteristic thermal hysteresis of the martensitic transition. Interestingly for **S4**, an increment in the magnetic contribution of the low temperature martensitic phase leads to the decrease in the magnetization change during the martensitic transformation. It is clearly observed how the martensitic transition temperature, T_{trans}, shifts from near-room temperature for **S1** to cryogenic temperatures for **S4**. Panel **(b)** illustrates the dependence with the Mn:Ni ratio of T_{trans} upon cooling and heating, calculated as the temperature of the maximum of dM/dT of the corresponding branch of the martensitic transition. It is common in Heusler alloys to find a linear dependence of the martensitic transition temperature with the electron per atom ratio (e/a), showing large changes in transformation temperatures upon minute variation in the e/a ratio [14,32,41,44]. For the studied alloy series, the e/a ratio decreases from 7.89 for **S1** to 7.86 for **S4**, leading to a decrease in transformation temperatures from 270 K (**S1**) to 120 K (**S4**) upon cooling. This drastic decrease in transformation temperatures upon minute decrease in the e/a ratio is recently reported for all-d-metal Ni(Co)-Mn-Ti Heusler alloy family: a decrease in e/a ratio of 0.12 for a series of alloys with similar compositions resulted in a decrease in transformation temperatures from ~ 430–145 K upon heating [25]. It is interesting to note that even with this large shift in T_{trans} from **S1** to **S4**, the magnetization of the austenitic phase remains almost unaltered. Previous studies have shown that the Co content is mainly responsible of Curie temperature variations in this family of alloys [32], which agrees with the observed invariant magnetic behavior of the austenite according to the constant Co content obtained by EDX results for the investigated alloys. The thermal hysteresis of each sample is obtained from the difference between the T_{trans} upon cooling and heating. A thermal hysteresis around 10 K is found for **S1**, **S2** and **S3** while a significant increase to 20 K is obtained for **S4**. This increase for **S4** is already observed for this system when approaching the cryogenic range due to the slower kinetics [25]. The value of thermal hysteresis obtained for **S3** of about 8 K is similar to some of other high-performance Ni(Co)-Mn-based Heusler alloys reported in the literature [45,46].

According to the results obtained from magnetization, the amount of austenitic phase at room temperature is expected to increase with the Mn:Ni ratio, in opposition to the results obtained from powder XRD. To clarify this, Fig. 4**c** shows the $M(T)$ plots upon heating for bulk and powder samples. It is evident that pulverizing the samples leads to a shift in T_{trans} towards higher temperatures with respect to the bulk ones. In accordance with the results obtained from XRD analysis at room temperature, it can be inferred from the $M(T)$ plots that powder **S1** and **S4** show majority of martensite whereas powder **S2** and **S3** show majority of austenite.

The isothermal entropy change as a function of temperature for magnetic field changes of 0.5, 1.0 and 1.5 T is plotted in Fig. 5**a**. All the alloys show large and sharp ΔS_{iso} responses, characteristic of materials undergoing FOPT. Furthermore, it can be noted that the position of the maximum of the isothermal entropy change shows a larger shift to lower temperatures with increasing field for **S4** in comparison to the other samples. This is ascribed to the larger transition temperature evolution with the magnetic field obtained for **S4** (−8 K/T) which is doubled in comparison to **S3**, **S2** and **S1** (−4 K/T). The peak values for 1.5 T (Fig. 5**b**) increases with increasing Mn:Ni ratio following a non-linear trend, reaching a maximumof 13 J kg^{-1} K^{-1} for both **S3** and **S4** samples. In addition, Fig. 5**c** shows the temperature average entropy change (TEC) plotted for the alloy series over a span of 5 K and 10 K, indicating that the TEC values for **S3** and **S4** are almost similar. Furthermore, the transition temperature for **S4** (120 K upon cooling) represents one of the lowest transformation temperatures for Ni-Mn based Heusler alloys [47]. This low working temperature for **S4** falls in the range of natural gas liquefaction. Furthermore, the observed ΔS_{iso} response for **S4** is almost 100% larger than that previously reported Ni(Co)-Mn-Ti samples with martensitic transition occurring in the cryogenic range [26]. Regarding hysteresis, the observed values for **S4** (Fig. 4**b**) are 20% reduced in comparison to those of the literature at the cryogenic range [25]. The reversible magnetocaloric response for the most favorable case, i.e., **S3** with the lowest thermal hysteresis, has been obtained from the overlapping of the heating and cooling branches of isothermal entropy changes at 1.5 T (inset of Fig. 5**a**) [48]. It should be highlighted that the cooling response is significantly smaller than the heating one. This is ascribed to the more gradual magnetization change upon the cooling branch of the martensitic transformation in comparison to the heating one (see Fig. 4**a**). The resulting reversible response, which is grey colored, has a maximum value of 5.1 J kg^{-1} K^{-1} for 1.5 T, corresponding to the 40% of the heating peak value of ΔS_{iso}. Although we have achieved a relevant reduction of the hysteresis of all-d-metal Heusler alloy systems for cryogenic applications with respect to

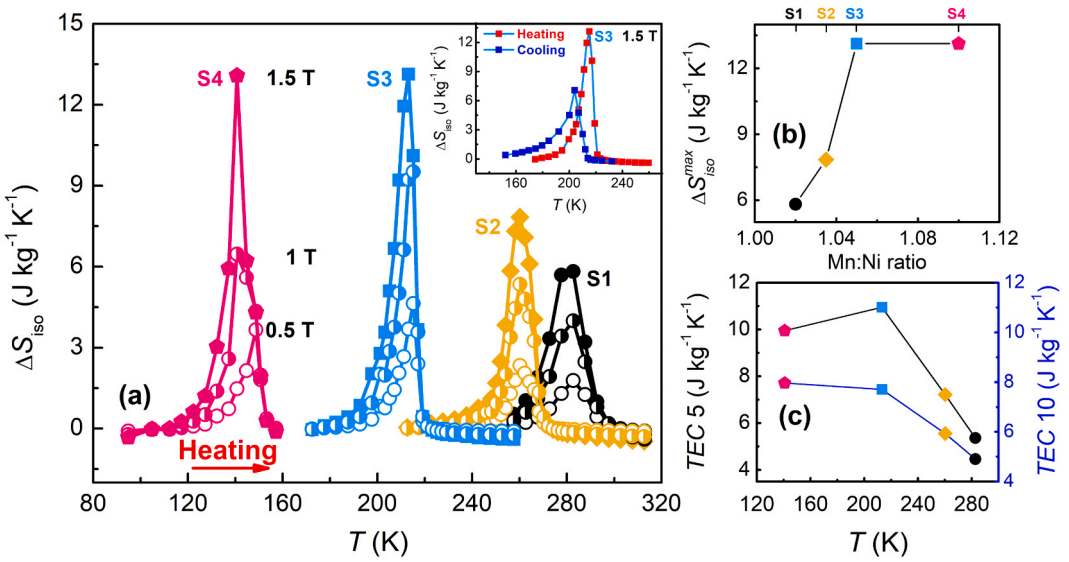

Fig. 5. (a) Temperature dependence of the heating isothermal entropy change at moderate magnetic fields. The inset shows the reversible magnetocaloric response for **S3**, (b) maximum isothermal entropy change (ΔS_{iso}^{max}) for 1.5 T and (c) temperature average entropy change (TEC) over a temperature span of 5 K and 10 K respectively for 1.5 T.

previous reports [25,26], further investigations and thorough material understanding directed towards further reduction of the thermal hysteresis is still required for improving the cyclic performance.

Besides high MCE, the material should show a proper balance between performance and criticality to be considered for final application. Fig. 6 draws a comparison between the ΔS_{iso} for the studied alloy series with reported magnetocaloric materials including Heusler alloy series [26,41,49–52], MM'X type [53] and, rare-earth based alloys [28–31] at the moderate magnetic field change of 1 T. In Fig. 6, the size of different symbols depicts their supply risk index values obtained using Ref. [20], where the alloy with lowest index is depicted with the smallest diameter. This index increases as the criticality of the material increases, where 1 is established as the threshold between non-critical and critical materials. It is observed that the studied alloy series shows index values around 1 for the series, which are rather low in comparison to the rare-earth containing alloys. Furthermore, **S4** shows a larger isothermal

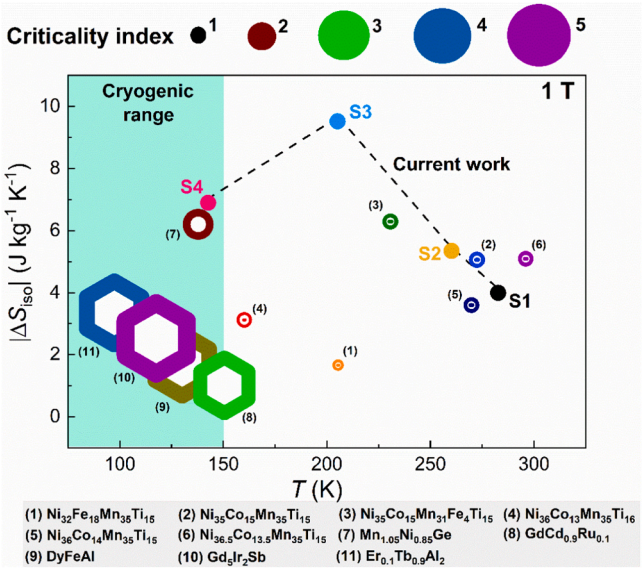

Fig. 6. |ΔS_{iso}| comparison between the investigated alloy series with various alloys reported in literature for 1 T. The size of the data points is proportional to their criticality index.

entropy change for 1 T than most of the materials reported in the literature for this temperature range [28–31,53]. This promising magnetocaloric performance together with relatively low criticality makes it a promising candidate for low-temperature applications.

4. Conclusions

The influence of the Mn:Ni ratio on the microstructure, martensitic transformation, and magnetocaloric performance of all-d-metal Ni(Co)-Mn-Ti Heusler alloys has been systematically investigated. The microstructural characterization reveals homogeneous compositions close to the nominal ones while depicting mixtures of austenite and martensite with minor presence of $L1_0$ structure for the studied series. The martensitic transition temperatures decrease from near-room temperature downwards cryogenic temperatures (120–140 K) as the Mn:Ni ratio increases. The magnetocaloric response is non-linearly increased as the transition temperature is shifted to lower temperatures. A large ΔS_{iso} of 13 J kg^{-1} K^{-1} for 1.5 T is obtained close to the natural gas liquefaction temperature for the sample with the highest Mn:Ni ratio. This response is double in comparison to that of recently reported Ni(Co)-Mn-Ti alloys at similar cryogenic temperatures. Together with relatively low criticality, these results open the possibility of considering this type of all-d-metal Heusler alloys also for cryogenic applications.

CRediT authorship contribution statement

Aun N. Khan: Methodology, Formal analysis, Investigation, Data Curation, Writing - Original Draft, Writing - Review & Editing. Á. Díaz-García: Methodology, Formal analysis, Investigation, Data Curation, Writing - Review & Editing. L. M. Moreno-Ramírez: Conceptualization, Methodology, Formal analysis, Investigation, Data. Curation, Writing - Review & Editing, Supervision. J. Y. Law: Conceptualization, Methodology, Formal analysis, Investigation, Writing - Review & Editing. V. Franco: Conceptualization, Methodology, Investigation, Writing - Review & Editing, Supervision, Funding acquisition.

Declaration of Competing Interest

The authors declare that they have no known competing financial interests or personal relationships that could have appeared to influence the work reported in this paper.

Data Availability

Data will be made available on request.

Acknowledgements

Work funded by PID2019–105720RB-I00/AEI/10.13039/501100011033. Additional funding from Air Force Office of Scientific Research (FA8655–21-1–7044) and the Clean Hydrogen Partnership and its members within the project HyLICAL (Grant no. 101101461) is also acknowledged. J.Y.L. acknowledges EMERGIA 2021 fellowship from Junta de la Andalucía (ref. EMC21_00418). ANK acknowledges a FPI fellowship from the Spanish MCIN/AEI.

References

[1] V. Franco, J.S. Blázquez, J.J. Ipus, J.Y. Law, L.M. Moreno-Ramírez, A. Conde, Magnetocaloric effect: from materials research to refrigeration devices, Prog. Mater. Sci. 93 (2018) 112–232, https://doi.org/10.1016/j.pmatsci.2017.10.005.
[2] J.Y. Law, L.M. Moreno-Ramírez, Á. Díaz-García, V. Franco, Current perspective in magnetocaloric materials research, J. Appl. Phys. 133 (2023) 40903, https://doi.org/10.1063/5.0130035.
[3] H. Zhang, R. Gimaev, B. Kovalev, K. Kamilov, V. Zverev, A. Tishin, Review on the materials and devices for magnetic refrigeration in the temperature range of nitrogen and hydrogen liquefaction, Phys. B. Condens. Matter 558 (2019) 65–73, https://doi.org/10.1016/j.physb.2019.01.035.
[4] O. Gutfleisch, V. Franco, Preface to the viewpoint set on: magnetic materials for energy, Scr. Mater. 67 (2012) 521–523, https://doi.org/10.1016/j.scriptamat.2012.07.012.
[5] A.M. Tishin, Y.I. Spichkin, The magnetocaloric effect and its applications, Mater. Today 6 (2003) 51, https://doi.org/10.1016/S1369-7021(03)01134-9.
[6] E. Stern-Taulats, A. Planes, P. Lloveras, M. Barrio, J.-L. Tamarit, S. Pramanick, S. Majumdar, S. Yüce, B. Emre, C. Frontera, L. Mañosa, Tailoring barocaloric and magnetocaloric properties in low-hysteresis magnetic shape memory alloys, Acta Mater. 96 (2015) 324–332, https://doi.org/10.1016/j.actamat.2015.06.026.
[7] O. Gutfleisch, T. Gottschall, M. Fries, D. Benke, I. Radulov, K.P. Skokov, H. Wende, M. Gruner, M. Acet, P. Entel, M. Farle, Mastering hysteresis in magnetocaloric materials, Philos. Trans. R. Soc. 374 (2016) 20150308, https://doi.org/10.1098/rsta.2015.0308.
[8] Á. Díaz-García, L.M. Moreno-Ramírez, J.Y. Law, F. Albertini, S. Fabbrici, V. Franco, Characterization of thermal hysteresis in magnetocaloric NiMnIn heusler alloys by temperature first order reversal curves (TFORC), J. Alloy. Compd. 867 (2021), 159184, https://doi.org/10.1016/j.jallcom.2021.159184.
[9] Yu.S. Koshkid'ko, E.T. Dilmieva, A.P. Kamantsev, J. Cwik, K. Rogacki, A. V. Mashirov, V.V. Khovaylo, C.S. Mejia, M.A. Zagrebin, V.V. Sokolovskiy, V. D. Buchelnikov, P. Ari-Gur, P. Bhale, V.G. Shavrov, V.V. Koledov, Magnetocaloric effect and magnetic phase diagram of Ni-Mn-Ga Heusler alloy in steady and pulsed magnetic fields, J. Alloy. Compd. 904 (2022), 164051, https://doi.org/10.1016/j.jallcom.2022.164051.
[10] T. Bachagha, J. Zhang, M. Khitouni, J. Suñol, NiMn-based Heusler magnetic shape memory alloys: a review, Int. J. Adv. Manuf. Technol. 103 (2019) 2761–2772, https://doi.org/10.1007/s00170-019-03534-3.
[11] H.Le Yan, H.X. Liu, Y. Zhao, N. Jia, J. Bai, B. Yang, Z. Li, Y. Zhang, C. Esling, X. Zhao, L. Zuo, Impact of B alloying on ductility and phase transition in the Ni–Mn-based magnetic shape memory alloys: insights from first-principles calculation, J. Mater. Sci. Technol. 74 (2021) 27–34, https://doi.org/10.1016/j.jmst.2020.10.010.
[12] S. Tavares, K. Yang, M.A. Meyers, Heusler alloys: past, properties, new alloys, and prospects, Prog. Mater. Sci. 132 (2023), 101017, https://doi.org/10.1016/j.pmatsci.2022.101017.
[13] Z.Y. Wei, E.K. Liu, Y. Li, X.L. Han, Z.W. Du, H.Z. Luo, G.D. Liu, X.K. Xi, H.W. Zhang, W.H. Wang, G.H. Wu, Magnetostructural martensitic transformations with large volume changes and magneto-strains in all-d-metal Heusler alloys, Appl. Phys. Lett. 109 (2016), 071904, https://doi.org/10.1063/1.4961382.
[14] V.G. de Paula, M.S. Reis, All-d-metal full Heusler alloys: a novel class of functional materials, Chem. Mater. 33 (2021) 5483–5495, https://doi.org/10.1021/acs.chemmater.1c01012.
[15] N.A. de Oliveira, P.J. von Ranke, Theoretical aspects of the magnetocaloric effect, Phys. Rep. 489 (2010) 89–159, https://doi.org/10.1016/j.physrep.2009.12.006.
[16] J. Ćwik, Y. Koshkid'ko, K. Nenkov, A. Mikhailova, M. Małecka, T. Romanova, N. Kolchugina, N.A. de Oliveira, Experimental and theoretical analysis of magnetocaloric behavior of Dy1-xErxNi2 intermetallics (x=0.25,0.5,0.75) and their composites for low-temperature refrigerators performing an Ericsson cycle, Phys. Rev. B. 103 (2021), 214429, https://doi.org/10.1103/PhysRevB.103.214429.
[17] J. Ćwik, Y. Koshkid'ko, K. Nenkov, E. Tereshina-Chitrova, M. Małecka, B. Weise, K. Kowalska, Magnetocaloric performance of the three-component Ho1-xErxNi2 (x = 0.25, 0.5, 0.75) Laves phases as composite refrigerants, Sci. Rep. 12 (2022), 12332, https://doi.org/10.1038/s41598-022-16738-7.
[18] X. Tang, H. Sepehri-Amin, N. Terada, A. Martin-Cid, I. Kurniawan, S. Kobayashi, Y. Kotani, H. Takeya, J. Lai, Y. Matsushita, T. Ohkubo, Y. Miura, T. Nakamura, K. Hono, Magnetic refrigeration material operating at a full temperature range required for hydrogen liquefaction, Nat. Commun. 13 (2022), 1817, https://doi.org/10.1038/s41467-022-29340-2.
[19] J. Ćwik, Y. Koshkid'ko, B. Weise, A. Czernuszewicz, High-field magnetic and magnetocaloric properties of pseudo-binary Er1−xHoxNi2 (x = 0.25–0.75) solid solutions, J. Alloy. Compd. 968 (2023), 172297, https://doi.org/10.1016/j.jallcom.2023.172297.
[20] G. Blengini, C. Latunussa, U. Eynard, C. Matos, K. Georgitzikis, C. Pavel, S. Carrara, L. Mancini, M. Unguru, D. Blagoeva, F. Mathieux, D. Pennington, Study on the EU's list of Critical Raw Materials Final Report, European Commission, 2020, https://doi.org/10.2873/11619.
[21] J. Lai, X. Tang, H. Sepehri-Amin, K. Hono, Tuning transition temperature of magnetocaloric Mn1.8Fe0.2(P0.59Si0.41) alloys for cryogenic magnetic refrigeration, Scr. Mater. 183 (2020) 127–132, https://doi.org/10.1016/j.scriptamat.2020.03.024.
[22] J. Lai, H. Sepehri-Amin, X. Tang, J. Li, Y. Matsushita, T. Ohkubo, A.T. Saito, K. Hono, Reduction of hysteresis in (La1-xCex) y(MnzFe11.4-z)Si1.6 magnetocaloric compounds for cryogenic magnetic refrigeration, Acta Mater. 220 (2021), 117286, https://doi.org/10.1016/j.actamat.2021.117286.
[23] J. Casey, B. Akintunde, R. Chandra Das, C. Hanley, B. Reese, M. Khan, A.K. Pathak, Anomalous magnetic entropy changes of bulk and powder Mn0.5Fe0.5-xNi1+xSi0.94Al0.06 intermetallic system, J. Magn. Magn. Mater. 579 (2023), 170862, https://doi.org/10.1016/j.jmmm.2023.170862.
[24] M. Khan, R.C. Das, J. Casey, B.L. Reese, B. Akintunde, A.K. Pathak, Near room temperature magnetocaloric properties in Ni deficient (Mn0.525Fe0.5) Ni0.975Si0.95Al0.05, AIP Adv. 12 (2022), 035227, https://doi.org/10.1063/9.0000294.
[25] B. Beckmann, D. Koch, L. Pfeuffer, T. Gottschall, A. Taubel, E. Adabifiroozjaei, O. N. Miroshkina, S. Riegg, T. Niehoff, N.A. Kani, M.E. Gruner, L. Molina-Luna, K. P. Skokov, O. Gutfleisch, Dissipation losses limiting first-order phase transition materials in cryogenic caloric cooling: a case study on all-d-metal Ni(-Co)-Mn-Ti Heusler alloys, Acta Mater. 246 (2023), 118695, https://doi.org/10.1016/j.actamat.2023.118695.
[26] Z. Guan, J. Bai, Y. Zhang, J. Gu, X. Liang, Y. Zhang, C. Esling, X. Zhao, L. Zuo, Simultaneously realized large low-temperature magnetocaloric effect and good mechanical properties in Ni36Co13Mn35Ti16 alloy, J. Appl. Phys. 131 (2022), 165107, https://doi.org/10.1063/5.0088692.
[27] N. ul Hassan, I.A. Shah, M. Jelani, M. Naeem, S. Riaz, S. Naseem, F. Xu, Z. Ullah, Effect of Ni-Mn ratio on structural, martensitic and magnetic properties of Ni-Mn-Co-Ti ferromagnetic shape memory alloys, Mater. Res. Expr. 5 (2018), 086102, https://doi.org/10.1088/2053-1591/aad124.
[28] M. Khan, K.A. Gschneidner Jr., V.K. Pecharsky, Magnetocaloric effects in Er1−xTbxAl2 alloys, J. Appl. Phys. 107 (2010), 09A904, https://doi.org/10.1063/1.3335590.
[29] K. Schäfer, C. Schwickert, O. Niehaus, F. Winter, R. Pöttgen, Magnetic properties of RE5Ir2X (RE = Y, Gd–Ho, X = Sn, Sb, Pb, Bi) and magnetocaloric characterization of Gd5Ir2X, Solid State Sci. 35 (2014) 66–73, https://doi.org/10.1016/j.solidstatesciences.2014.06.010.
[30] L. Li, D. Huo, Z. Qian, K. Nishimura, Study of the critical behaviour and magnetocaloric effect in DyFeAl, Intermetallics 46 (2014) 231–235, https://doi.org/10.1016/j.intermet.2013.11.019.
[31] L.-W. Li, Review of magnetic properties and magnetocaloric effect in the intermetallic compounds of rare earth with low boiling point metals, Chin. Phys. B. 25 (2016), 037502, https://doi.org/10.1088/1674-1056/25/3/037502.
[32] A. Taubel, B. Beckmann, L. Pfeuffer, N. Fortunato, F. Scheibel, S. Ener, T. Gottschall, K.P. Skokov, H. Zhang, O. Gutfleisch, Tailoring magnetocaloric effect in all-d-metal Ni-Co-Mn-Ti Heusler alloys: a combined experimental and theoretical study, Acta Mater. 201 (2020) 425–434, https://doi.org/10.1016/j.actamat.2020.10.013.
[33] A.N. Khan, L.M. Moreno-Ramírez, Á. Díaz-García, J.Y. Law, V. Franco, All-d-metal Ni(Co)-Mn(X)-Ti (X = Fe or Cr) Heusler alloys: Enhanced magnetocaloric effect for moderate magnetic fields, J. Alloy. Compd. 931 (2023), 167559, https://doi.org/10.1016/j.jallcom.2022.167559.
[34] V.K. Pecharsky, K.A. Gschneidner Jr, Magnetocaloric effect and magnetic refrigeration, J. Magn. Magn. Mater. 200 (1999) 44–56, https://doi.org/10.1016/S0304-8853(99)00397-2.
[35] J.S. Amaral, V.S. Amaral, On estimating the magnetocaloric effect from magnetization measurements, J. Magn. Magn. Mater. 322 (2010) 1552–1557, https://doi.org/10.1016/j.jmmm.2009.06.013.
[36] L. Tocado, E. Palacios, R. Burriel, Entropy determinations and magnetocaloric parameters in systems with first-order transitions: Study of MnAs, J. Appl. Phys. 105 (2009), 093918, https://doi.org/10.1063/1.3093880.
[37] L. Caron, Z.Q. Ou, T.T. Nguyen, D.T. Cam Thanh, O. Tegus, E. Brück, On the determination of the magnetic entropy change in materials with first-order transitions, J. Magn. Magn. Mater. 321 (2009) 3559–3566, https://doi.org/10.1016/j.jmmm.2009.06.086.
[38] V. Franco, Magnetocaloric characterization of materials. Magnetic Measurement Techniques for Materials Characterization, Springer International Publishing, Cham, 2021, pp. 697–726, https://doi.org/10.1007/978-3-030-70443-8_23.
[39] L.M. Moreno-Ramírez, J.J. Ipus, V. Franco, J.S. Blázquez, A. Conde, Analysis of magnetocaloric effect of ball milled amorphous alloys: Demagnetizing factor and Curie temperature distribution, J. Alloy. Compd. 622 (2015) 606–609, https://doi.org/10.1016/j.jallcom.2014.10.134.
[40] L.D. Griffith, Y. Mudryk, J. Slaughter, V.K. Pecharsky, Material-based figure of merit for caloric materials, J. Appl. Phys. 123 (2018), 034902, https://doi.org/10.1063/1.5004173.

[41] Z. Guan, X. Jiang, J. Gu, J. Bai, X. Liang, H. Yan, Y. Zhang, C. Esling, X. Zhao, L. Zuo, Large magnetocaloric effect and excellent mechanical properties near room temperature in Ni-Co-Mn-Ti non-textured polycrystalline alloys, Appl. Phys. Lett. 119 (2021) 51904, https://doi.org/10.1063/5.0058609.
[42] H. Neves Bez, A.K. Pathak, A. Biswas, N. Zarkevich, V. Balema, Y. Mudryk, D. D. Johnson, V.K. Pecharsky, Giant enhancement of the magnetocaloric response in Ni–Co–Mn–Ti by rapid solidification, Acta Mater. 173 (2019) 225–230, https://doi.org/10.1016/j.actamat.2019.05.004.
[43] S. Singh, P. Kushwaha, F. Scheibel, H.-P. Liermann, S.R. Barman, M. Acet, C. Felser, D. Pandey, Residual stress induced stabilization of martensite phase and its effect on the magnetostructural transition in Mn-rich Ni-Mn-In/Ga magnetic shape-memory alloys, Phys. Rev. B. 92 (2015) 20105, https://doi.org/10.1103/PhysRevB.92.020105.
[44] T. Bachagha, J.-J. Suñol, All-d-metal Heusler alloys: a review, Metals 13 (2023) 111, https://doi.org/10.3390/met13010111.
[45] R. Millán-Solsona, E. Stern-Taulats, E. Vives, A. Planes, J. Sharma, A.K. Nayak, K. G. Suresh, L. Mañosa, Large entropy change associated with the elastocaloric effect in polycrystalline Ni-Mn-Sb-Co magnetic shape memory alloys, Appl. Phys. Lett. 105 (2014), 241901, https://doi.org/10.1063/1.4904419.
[46] T. Chabri, A. Barman, S. Chatterjee, S.A. Mollick, T.K. Nath, D. Mukherjee, Effects of transitional hysteresis on the large magnetocaloric and magnetoresistance properties of Ni-Mn-Co-Sn Heusler alloy, J. Alloy. Compd. 863 (2021), 158485, https://doi.org/10.1016/j.jallcom.2020.158485.
[47] T. Gottschall, K.P. Skokov, D. Benke, M.E. Gruner, O. Gutfleisch, Contradictory role of the magnetic contribution in inverse magnetocaloric Heusler materials, Phys. Rev. B. 93 (2016), 184431, https://doi.org/10.1103/PhysRevB.93.184431.
[48] E. Stern-Taulats, A. Planes, P. Lloveras, M. Barrio, J.-L. Tamarit, S. Pramanick, S. Majumdar, C. Frontera, L. Mañosa, Barocaloric and magnetocaloric effects in Fe49Rh51, Phys. Rev. B. 89 (2014), 214105, https://doi.org/10.1103/PhysRevB.89.214105.
[49] Z.Y. Wei, E.K. Liu, J.H. Chen, Y. Li, G.D. Liu, H.Z. Luo, X.K. Xi, H.W. Zhang, W. H. Wang, G.H. Wu, Realization of multifunctional shape-memory ferromagnets in all-d-metal Heusler phases, Appl. Phys. Lett. 107 (2015), 022406, https://doi.org/10.1063/1.4927058.
[50] Q. Zeng, J. Shen, H. Zhang, J. Chen, B. Ding, X. Xi, E. Liu, W. Wang, G. Wu, Electronic behaviors during martensitic transformations in all-d-metal Heusler alloys, J. Phys.: Condens. Matter 31 (2019), 425401, https://doi.org/10.1088/1361-648X/ab2bd8.
[51] K. Liu, S. Ma, C. Ma, X. Han, K. Yu, S. Yang, Z. Zhang, Y. Song, X. Luo, C. Chen, S. U. Rehman, Z. Zhong, Martensitic transformation and giant magneto-functional properties in all-d-metal Ni-Co-Mn-Ti alloy ribbons, J. Alloy. Compd. 790 (2019) 78–92, https://doi.org/10.1016/j.jallcom.2019.03.173.
[52] Y. Li, L. Qin, S. Huang, L. Li, Enhanced magnetocaloric performances and tunable martensitic transformation in Ni35Co15Mn35−xFexTi15 all-d-metal Heusler alloys by chemical and physical pressures, Sci. China Mater. 65 (2022) 486–493, https://doi.org/10.1007/s40843-021-1747-3.
[53] C.L. Zhang, D.H. Wang, Q.Q. Cao, Z.D. Han, H.C. Xuan, Y.W. Du, Magnetostructural phase transition and magnetocaloric effect in off-stoichiometric Mn1.9−xNixGe alloys, Appl. Phys. Lett. 93 (2008), 122505, https://doi.org/10.1063/1.2990649.